THE EFFECT OF REINFORCEMENT ARCHITECTURE ON THE LONG RANGE FLOW IN FIBROUS REINFORCEMENTS

3rd Int. Conf. Flow Processes in Composite Materials, Galway, July 1994.

P R Griffin (a); S M Grove (a); F J Guild (b); P Russell (c); D Short (a); J Summerscales (a); and E Taylor (d).

(a) School of Manufacturing, Materials and Mechanical Engineering
University of Plymouth, Plymouth, Devon PL4 8AA.

(b) Department of Materials Science and Engineering
University of Surrey, Guildford, Surrey, GU2 5XH.

(c) Department of Biological Sciences
University of Plymouth, Plymouth, Devon PL4 8AA.

(d) Carr Reinforcements Limited
Heapriding Business Park, Chestergate, Stockport, SK3 0BT.

Abstract

The resin transfer moulding process involves the long range flow of resin into a closed mould which is filled with dry fibre reinforcement. The rate of resin flow can be calculated using the Darcy and Kozeny-Carman equations. The flow rate is thus a function of the pressure drop across the fibre bed, the resin viscosity and the permeability of the fibre bed. The permeability constant is dependent on the fibre radius and the porosity of the bed.

A number of reinforcement fabrics are now available commercially which promote faster resin flow than that in equivalent fabrics of the same areal weight at the same fibre volume fraction. The Kozeny-Carman equation includes a parameter known as the mean hydraulic radius. If this parameter is varied by calculating a specific hydraulic radius, then the flow enhancement may be modelled. Calculations for model materials have been published and demonstrate that this approach predicts that significant changes in flow rate are possible.

The commercial fabrics do not have model structures, but feature variations in the mesoscale architecture of the reinforcement: fibres clustered into tows and uneven distribution of pore space. The paper will report on the correlation of quantitative image analysis of optical micrographs with the flow rates in a range of reinforcement fabrics.

Introduction

Resin transfer moulding (RTM) is a process for producing fibre-reinforced polymeric parts in final shape. A dry preform of reinforcement fibres is placed into a net-shape mould, which is closed before resin is injected into the mould to fill the spaces between the fibres. Once the resin has cured, the stiff solid composite component can be removed from the mould. Unlike all other composite manufacturing processes, RTM involves long-range flow of resin through the porespace between the reinforcement fibres. The process and the associated governing equations have been well described [1-3].

The one-dimensional flow of fluid through a porous bed was modelled by Darcy [4] in 1856. Darcy's law relates the linear flow rate, q, to a coefficient depending on the permeability, K, the pressure drop, ΔP, and the bed length, L, through the equation:

$$q = \frac{K.\Delta P}{L} \qquad \text{..... (1)}$$

Kozeny [5] and Carman [6] considered the relationship between the volumetric flow rate of fluid, Q, and the porosity (fractional free volume in the bed), ε, and found it to be governed by the equation:

$$Q = \frac{A\varepsilon.m^2}{k\mu}.\frac{\Delta P}{L} \qquad \text{..... (2)}$$

where A is the cross-sectional area of the bed, k is the Kozeny constant, m is the mean hydraulic radius of the bed, and μ is the dynamic viscosity of the fluid.

The concept of the hydraulic radius of the bed is attributed to Blake [7], and is defined as the cross-sectional area normal to the flow divided by the perimeter presented to the fluid. Williams et al [8] suggested that the mean hydraulic radius of a unidirectional fibre bed is given by Equation 5:

$$m = \frac{r}{2}.\frac{\varepsilon}{(1-\varepsilon)} = \frac{rV_m}{2V_f} \qquad \text{..... (3)}$$

where r is the fibre radius, V_m is the matrix volume fraction of the void-free composite and V_f is the fibre volume fraction. Hence:

$$\varepsilon = V_m = (1 - V_f) \qquad \text{..... (4)}$$

The 1-D volumetric flow rate can be represented by Darcy's equation by including the cross sectional area normal to the flow on both sides of the equation, hence:

$$Q = q.A = KA.\frac{\Delta P}{L} \qquad \text{..... (5)}$$

and substituting Equation 3 into Equation 2 gives:

$$Q = \frac{Ar^2}{4k\mu}.\frac{\varepsilon^3}{(1-\varepsilon)^2}.\frac{\Delta P}{L} \qquad \text{..... (6)}$$

Equating the right hand sides of Equations 5 and 6 gives:

$$K = \frac{r^2\varepsilon^3}{4k\mu(1-\varepsilon)^2} \qquad \text{..... (7)}$$

Thirion et al [9] have demonstrated that the linear flow rate through the same volume fraction of similar reinforcement fibres with different reinforcement architectures under identical flow conditions was more rapid in fabrics with clustered tows. Griffin [10] has conducted a comprehensive survey of international studies of the permeability of fibrous reinforcements and found that reported values for similar fabrics might vary by one or two orders of magnitude. Griffin and Grove [11] have reported that the rate of flow front advance increased with the proportion of spiral-bound tows at constant reinforcement volume fraction.

Clearly Equation 7 is only applicable to situations in which we might expect the fibres to be organised such that the **mean** hydraulic radius is an applicable concept. This situation is only likely to be relevant when the fibres are organised with uniform or truly random packing. The use of weaving techniques to produce commercially useful reinforcement will inevitably organise the reinforcement tows into clustered groups.

Summerscales has analysed situations with clustered fibres [12] and clustered layers [13] to determine the effect of variations in the reinforcement architecture on the flow rate. The predicted flow rate in a regular array of clustered fibres was significantly increased relative to a uniform distribution of individual fibres at the same volume fraction. Similarly, the flow rate is predicted to be higher in a small number of thick layers when compared to a large number of thin layers.

The materials analysed by Summerscales were idealised models. The evaluation of real materials will require the use of automated microstructural image analysis. The use of such techniques for fibre-reinforced composites has been reviewed by Guild and Summerscales [14].

Quantitative microscopy, using spatial statistics, is capable of revealing subtle relationships amongst the fibres in the composite. Summerscales et al [15] used the Voronoi half-interparticle distance to characterise the microstructure of carbon fibre-reinforced plastics processed by the vacuum-bag technique using different process dwell times.

Li et al [16] used automatic image analysis to quantitatively evaluate fibre distributions in cast continuous aligned aluminia fibre-reinforced aluminium alloy. Significant differences could not be detected between the fibre distributions of samples solidified under different conditions.

Everett and Chu [17] modelled the microstructural effects of non-uniform composite microstructures. Fibre positions and areas were determined from micrographs of Nicalon (SiC)/zirconia titanate ceramic by image analysis, or were generated by a computer program. Dirichlet cell tesselations, number of cell sides, cell volume fraction and nearest-neighbour distances were calculated. The flexural strength of the ceramic matrix composites which exhibited clustering was found to correlate with the maximum value of nearest-neighbour distance distribution skewness.

Experimental Techniques

Materials Used:

The carbon-fibre reinforcement fabrics in this study were developed by Carr Reinforcements with the specific aim of promoting resin flow. All fabrics were 2 x 2 twill weaves, with from 0-7 flow-enhancing warp threads to each normal warp tow. The materials used are summarised in Table 1.

TABLE 1: Materials used in the experimental study

REINFORCEMENT FABRICS		
Designation	**Description**	**% Bound Tows**
38166	normal 2 x 2 twill weave	0%
156	one bound tow in each eight tows	12.5%
150	one bound tow in each six tows	16.7%
148	one bound tow in each four tows	25%
126	one bound tow in each two tows	50%
FLUIDS		
Boots glycerol		
BDH glycerol		
Scott Bader unsaturated polyester resin A cured with MEKP		
Scott Bader unsaturated polyester resin E cured with MEKP		
Jotun Polymer unsaturated polyester resin 4210 cured with MEKP		
Jotun Polymer unsaturated polyester resin 4210 cured with AAP		

Permeability measurements and composite manufacture

Four layers of one type of fabric were laid up in a 350 mm square 1.7 mm deep parallel-sided flat mould. The fabrics are anisotropic due to the inclusion of the bound flow-enhancing warp thread. To measure the permeability in quasi-isotropic flow, the layer stacking sequence was $[0/90]_s$ and a fluid inlet port was included at the centre of the lower face of the mould. A central hole (diameter of 14 mm) was punched in the centre of each fabric layer to encourage true two-dimensional flow throughout the permeability experiment.

The flow fluid was introduced through the central inlet port into the space punched into the reinforcement layers. The fluid pressure at the reservoir was 0.9 bar gauge pressure (ie 1.9 bar pressure absolute). The fluid permeated radially outwards. The flow front isochrones were recorded at 30 second intervals during the early stages and one minute intervals in the later stages of each flow experiment. The permeability values were calculated using the radial form of Darcy's law. This approach is similar to that of Adams et al [18] and Hwang and Chang [19].

Further experiments were conducted using an anisotropic stacking sequence, $[0_2]_s$ under the same conditions as above.

The permeability results using Boots glycerol are shown in Figure 1. Since the experiments were performed, we have become aware of the high variability in the measured viscosity of glycerol [20]. All fabrics had similar areal weights (a range of 5g/m^2 for a nominal fabric weight of 382 g/m^2). All experiments were conducted in the same mould, to the same nominal thickness, and hence at equivalent volume fractions. The permeability increased with the number of flow-enhancing tows. This result would not be predicted by Kozeny-Carman law as volume

fractions (porosities) were nominally identical and a mean hydraulic radius is used in that equation (equation 2).

Figure 2 summarises the permeability results for the full range of fluids used (listed in Table 1). All experiments were conducted under identical conditions, except for the fluids and their viscosities, and hence it would not be expected that different permeabilities resulted. A similar problem has been reported by Steenkamer et al [21]. The explanation may be that the experimental configuration involves the wetting of fabric (unlike Darcy's original wetted flow experiment) and hence surface chemistry/physics may assume a significant importance. The flow regime could also involve extensional flow, rather than bulk flow, and the different performance of each flow fluid in this regime could be critical.

The procedure used follows that developed by Griffin [22-24]. The full mathematical derivation of the model has been reported by Carter et al [25]. A standard experimental apparatus and procedure have been proposed by Fell et al [26].

Microstructural Examination

Sections perpendicular to the flow-enhancing fibre direction were cut from the anisotropic plates at 20, 40 and 60 mm from the inlet position normal to the bound tow. The sections were mounted in casting resin. The sections were polished on 'wet-and-dry' diamond papers of 200, 320, 400 and 600 grade in turn, until the surface appeared flat to the unaided eye. The sections were then polished using an automatic metallurgical polishing machine with diamond pastes and a specimen load of 1 kg. The sequence used was: 1 h at 14 μm; 1 h at 6 μm; 30 min at 1 μm; and a final short polish at 0.25 μm.

The microstructure of a unidirectional continuous-fibre composite is entirely defined by sections perpendicular to the fibre direction, assuming that the fibres are perfectly straight and of constant cross-section along their length. The samples examined are reinforced with bidirectional (orthogonal) fabrics. The flow direction fibres appear as circles and the transverse fibres lie in the plane of the section. The sections were examined with a Quantimet 570 Automatic Image Analyser. The section was placed in bright-field illumination in the microscope. The overall magnification used was recorded for each individual frame, typically 0.0162-0.0178 mm/pixel.

The features of the Quantimet 570 used in this work will be briefly described. The maximum size of frame which can be examined is divided into a square grid of 512 x 512 square pixels. The contrast is divided into 256 grey levels; black is defined as grey level 0 and white is defined as grey level 255. The grey level of each pixel is recorded as an 8-bit digital word. Detection was carried out with respect to a single threshold. The threshold level and detection were set so that the carbon fibres appeared white with respect to the matrix. Figure 3 is a grey-level image of a typical section. The fibre bundles are darker than the flow space. Individual fibres are not detected at this magnification. The flow areas could thus be detected as features, and their centres of gravity, i.e., their x, y coordinates with respect to the frame, could be measured and recorded. The image-enhancement processing of the Quantimet is used to improve the image after converting the image to a binary form.

The microstructure of the laminate is variable due to its construction using carbon fibres in tows; measurements must be taken over an area which reflects the size of this variability. The total area analysed was a grid of 3 contiguous frames in the sample width, parallel to the weft direction. The measure frame used was 438 x 123 pixels: for sample 156 this corresponds to 21.3 mm wide by 1.99 mm high total area analysed.

The image shown in Figure 4 is a binary image; each pixel is defined as detected or not detected. The sophisticated image processing available on the Quantimet 570 arises from its large storage capacity. Such image enhancement was used here; the 'segment' process was used. This essentially consists of successive erosions and builds (dilations without remerge) of features, leading to their separation. Figure 5 shows the binary image of the same field after the image enhancement. The flow areas are now detected as separate features.

The process of image capture, image processing, measurement and movement of the stored image to prepare for the next frame was programmed using QBASIC, the command language of the Quantimet. The results were written onto a floppy disk; for each fibre-free zone, the parameters recorded were area, maximum feature height (vertical feret) and maximum feature width (horizontal feret), x- and y- centres of gravity and perimeter. The results were subsequently analysed using a spreadsheet (LOTUS 1-2-3).

The data was divided into bins from which histograms can be drawn. An alternative presentation of the data is a continuous plot showing the total number in a given range and all smaller ranges. Results from different laminates are more easily compared using such continuous plots. Comparisons can be made if the total number is normalised; the y-axis range is 0 to 1. These are plots of the cumulative distribution function.

Results and Discussion

The permeability of the reinforcement fabrics at constant (to within ± 2%) volume fraction increase with the proportion of (bound) flow-enhancing tows. The values are calculated from each of the flow front isochrones recorded using the radial form of Darcy's equation, and the values reported in Table 2 are the averages of at least ten values.

TABLE 2 : Permeability values determined with Boots glycerol

Fabric Number:	38166	156	150	148	126
Description:	Twill	12% bound	17% bound	25% bound	50% bound
Permeability: ($\times 10^{-12}$ m^2)	25.6	149	180	206	208

Tests were run on fabric 126 using a variety of flow fluids. The permeabilities calculated were dependent on the flow fluid (Table 3) which confirms the findings of Steenkamer et al [21].

TABLE 3: Variation of permeability with flow fluid for fabric 126

Flow Fluid:	BDH glycerol	Boots glycerol	Scott Bader Resin E
Mean permeability ($\times 10^{-12}$ m^2)	165	208	1288

It proved impractical to undertake the quantitative microscopy of samples manufactured with two of the fabrics (150 and 148), because the samples were damaged during preparation. The sum of the microstructure parameters measured are recorded in Table 4.

TABLE 4: Total areas and perimeters of voids determined by quantitative microscopy

Fabric No.	Total no of areas	Total area (mm^2)	Total perimeter (mm)	Av perimeter area (mm)
126	130	11.21	146.4	1.126
156	115	8.54	112.4	0.977
Twill	210	5.47	139.6	0.655

The Blake-Kozeny-Carman (BKC) equation predicts that flow will be proportional to total area wetted per unit volume or to total perimeter wetted per unit area. The "areas" reported in Table 4 are the areas of the large pore space (voids in the unwetted reinforcement) and not the areas corresponding to the BKC equation. A threshold pore space area of ~5 pixels was set to eliminate the small pore spaces corresponding to close packing of the fibres as flow visualisation experiments [27] suggest that flow occurs in the macro-porosity of the reinforcement.

The perimeters recorded do correspond to those of the BKC equation. However, it is not yet practical to determine the effective penetration of the flow front into the tows during wetting, so a global perimeter has been determined from the large areas in isolation.

The parameters determined in Table 4 have been plotted as histograms. The results are reported in more detail elsewhere [28]. The middle-range flow areas are more abundant in fabric 126 (which has most flow enhancing tows) and least abundant in the twill fabric. The flow enhancing tow can therefore be seen to achieve the required effect by creating flow passages, which are predominantly in the range ~> 0.6 mm^2. These areas are of irregular shape and hence the ratio of perimeter to area is variable. The total perimeters in Table 4 do not correspond to the expectations of the BKC equation. The perimeters which correspond to the above middle-range flow areas are summarised in Table 5. The resolution of these perimeters is limited by the pixel size and by the diffuse edges of the large flow areas due to the separation of individual fibres along the tow edge. Further study of the perimeter as a factor determining the flow will require examination of this parameter over a range of magnifications.

TABLE 5: Sum of perimeters of large flow areas in millimetres. (number of areas considered)

	Twill	156	126
Area >0.4mm^2	86.6 (47)	31.6 (34)	95.6 (41)
Area >0.6 mm^2	69.9 (32)	31.0 (23)	86.6 (30)
Area >0.8 mm^2	61.2 (24)	30.7 (18)	80.0 (25)
Area >1.0 mm^2	59.6 (23)	30.6 (17)	76.2 (22)

The histograms of zone area for the three laminates are shown in Figure 6. The highest bin used is 0.15 mm^2. The final bin includes all areas greater than the size of the highest bin. Histograms for these large areas are shown in Figure 7. The larger total number of areas measured for the twill (Table 4) is clear from the histogram; the larger total number arises from larger numbers of small areas. Comparing Figures 7a, b and c, it is clear that the introduction of the twisted tows allows more large areas to occur. The number and distribution of these large areas are not significantly changed by changing the frequency of the twisted tows (Figures 7b and c). The effect of the twisted tows on the intermediate areas is not clear from comparison of these histograms.

The dimensions of the fibre-free zones were compared using cumulative plots. Figure 8 shows the plots of the total number; Figure 9 shows the plots where the total number has been normalized. As expected from the overall laminate construction, the values of through-thickness length (Figures 8 and 9a) are smaller than the values of in-plane length (Figures 8 and 9b); the x-axes are different lengths for each direction. Considering first the plots of 'Total Number', Figure 8: the ranking of the graphs for very small lengths is the ranking expected from the number of twisted tows. Increasing the number of twisted tows leads to a decrease in the number of small zone lengths. The difference is clearer for the through-thickness length (Figure 8a). However, the plots for the 156 and 126 laminates cross since the 126 laminate had a higher overall number of zones (Table 4). The difference between the laminates is clarified by the normalisation (Figure 9). The ranking remains unchanged throughout the range. The 126 laminate has the lowest proportion of small dimensions, that is the highest proportion of long dimensions. The effect is most apparent in the through-thickness direction.

Summary

Permeability experiments have been conducted on a series of fabrics containing a variable number of flow enhancing tows. The permeability was found to be dependent on the flow fluid used, but values for a single fluid showed the expected increase in permeability with number of flow enhancing tows. Quantitative microscopy revealed that flow enhancement was accompanied by the presence of large flow areas adjacent to the "bound" tows and increased in line with the average perimeter of these areas.

References

1. K VAN HARTEN
"Production by resin transfer moulding"
Chapter 4 of RA Shenoi and J F Wellicome (editors):
"Composite Materials in Maritime Structures", CUP, Cambridge, 1993, pp 86-126

2. C L TUCKER and R B DESSENBERGER
"Governing Equations for Flow and Heat Transfer in Stationary Fibre Beds"
Chapter 8 of SG Advani (editor):
"Flow and Rheology in Polymer Composites Manufacturing", Elsevier, Amsterdam, 1994, pp 257-323

3. S G ADVANI and M V BRUSCHKE
"Resin Transfer Moulding Phenomena in Polymeric Composites"
Chapter 12 of S G Advani (editor):
Ibid, pages 465-515

4. H P G DARCY
"Les fontaines publiques de la ville de Dijon"
Dalmont, Paris, 1856.

5. J KOZENY
"Uber die Kapillare Leitung des Wassers in Boden""
Sitzungsberichte Akademie der Wissenschaft Wien Math-naturw, 1927, 136 (Kl.abt.IIa), 271-306.

6. P C CARMAN
"Fluid flow through a granular bed"
Transactions of the Institute of Chemical Engineers (London), 1937, 15, 150-166.

7. F C BLAKE
"The resistance of packing to fluid flow"
Transactions of the American Institute of Chemical Engineers, 1922, 14, 415-421.

8. J G WILLIAMS, CEM MORRIS and B C ENNIS
"Liquid flow through aligned fibre beds"
Polymer Engineering and Science, June 1974, 14(6), 413-419.

9. J M THIRION, H GIRARDY and U WALDVOGEL
"New developments in resin transfer moulding of high-performance composite parts"
Composites (Paris), 1988, 28(3), 81-84.

10. P R GRIFFIN
"Reinforcement permeability values - a brief review"
University of Plymouth report BE5477/UoP/BE/1.2/D/CC/1.0, December 1993

11. P R GRIFFIN and S M GROVE
"Measurements of Permeability of Fibre Reinforcements: A Review"
In preparation

12. J SUMMERSCALES
"A model for the effect of fibre clustering on the flow rate in resin transfer moulding"
Composites Manufacturing, 1993, 4(1), 27-31.

13. J SUMMERSCALES, E J CARTER and A W FELL
"A model for the effect of layer clustering and layer porosity on the flow rate in resin transfer moulding"
Composites Manufacturing, in submission.

14. F J GUILD and J SUMMERSCALES
"Microstructural image analysis applied to fibre composite materials"
Composites, 1993, 24(5), 383-394.

15. J SUMMERSCALES, D GREEN and F J GUILD
"Effect of processing dwell-time on the microstructure of a fibre reinforced composite"
Journal of Microscopy, February 1993, 169(2), 173-182.

16. Q F LI
"Quantitative evaluation of fibre distributions in a continuously reinforced aluminium alloy using automatic image analysis"
Materials Characterisation, 1992, 28(3), 189-203.

17. R K EVERETT and J H CHU
"Modelling of non-uniform composite microstructures"
Journal of Composite Materials, 1993, 27(11), 1128-1144.

18. K L ADAMS, W B RUSSEL and L REBENFELD
"Radial penetration of a viscous fluid into a planar anisotropic porous medium"
International Journal of Multiphase Flow, 1988, 14(2), 203-215.

19. A W CHAN and S HWANG
"Anisotropic in-plane permeability of fabric media"
Polymer Engineering and Science, 1991, 31(16), 1233-1239.

20. P N SHANKAR and M KUMAR
"Experimental determination of the kinematic viscosity of glycerol-water mixtures"
Proc Roy Soc London, 8 March 1994, A444(1922), 573-581

21. D A STEENKAMER, D J WILKINS and V M KARBHARI
"Influence of test fluid on fabric permeability measurements and implications for processing of liquid moulded composites"
Journal of Materials Science Letters, 1 July 1993, 12 (13), 971-973

22. P R GRIFFIN
"RTM flow visualisation and quantification"
BEng project report, Polytechnic South West, May 1990.

23. P R GRIFFIN
"Measurement of permeability of reinforcement fabrics to resin flow"
Advanced Composites Manufacturing Centre Report, February 1991.

24. P R GRIFFIN
"Simulation and Optimisation of the Resin Transfer Moulding Process"
MPhil/PhD Transfer Report, University of Plymouth, 1993

25. E J CARTER, A W FELL and J SUMMERSCALES
"The permeability of reinforcement fabrics, Part 1:
A simplified model for the derivation of the permeability tensor of an anisotropic fibre bed"
Composites Manufacturing, in submission.

26. A W FELL, E J CARTER and J SUMMERSCALES
"The permeability of reinforcement fabrics, Part 2:
A proposed standard experimental apparatus and procedure"
Composites Manufacturing, in preparation.

27. P R GRIFFIN, S M GROVE, A LEWIS and D SHORT
"Flow visualisation in resin transfer moulding"
This conference

28. P R GRIFFIN, S M GROVE, F J GUILD, P RUSSELL, D SHORT, J SUMMERSCALES and E TAYLOR
"The Effect of Microstructure on Flow Promotion in RTM Reinforcement Fabrics"
Journal of Microscopy, in submission

Figure 1. Permeability of Glycerol (supplied by Boots) through a Range of Flow Enhancing Reinforcement Fabrics

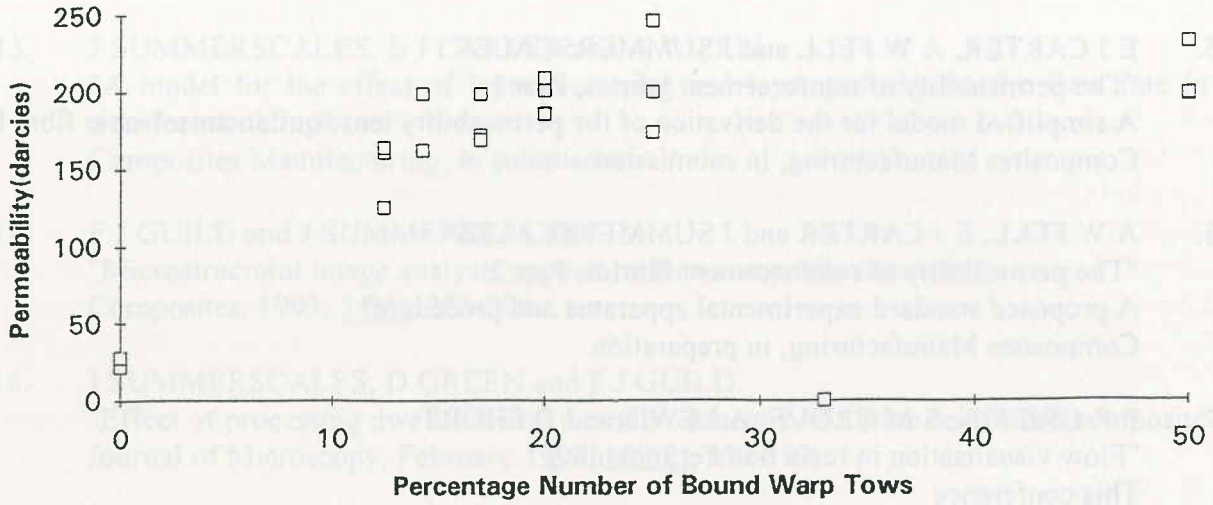

Figure 2. Permeability of a Range of Flow Enhancing Reinforcements to Various Test Fluids

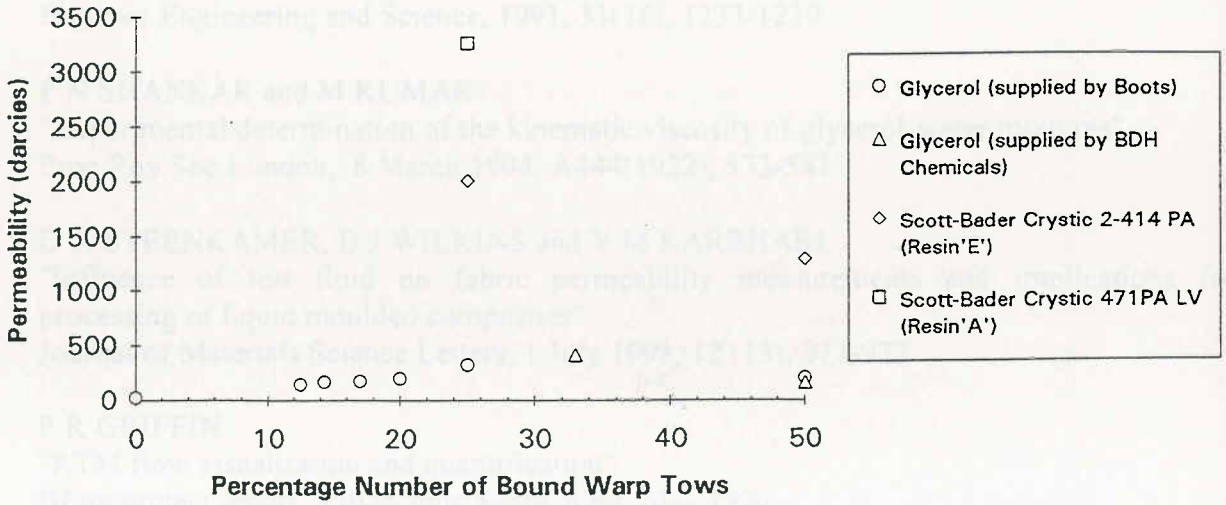

Figure 3. A Grey level Detection of a Section of a Fabric 156 Laminate

Figure 4. A Binary Image of the Fabric 156 Laminate

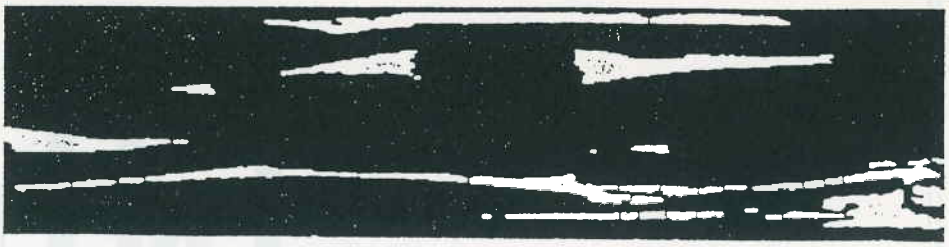

Figure 5. The Section of 156 Fabric after Image Enhancement

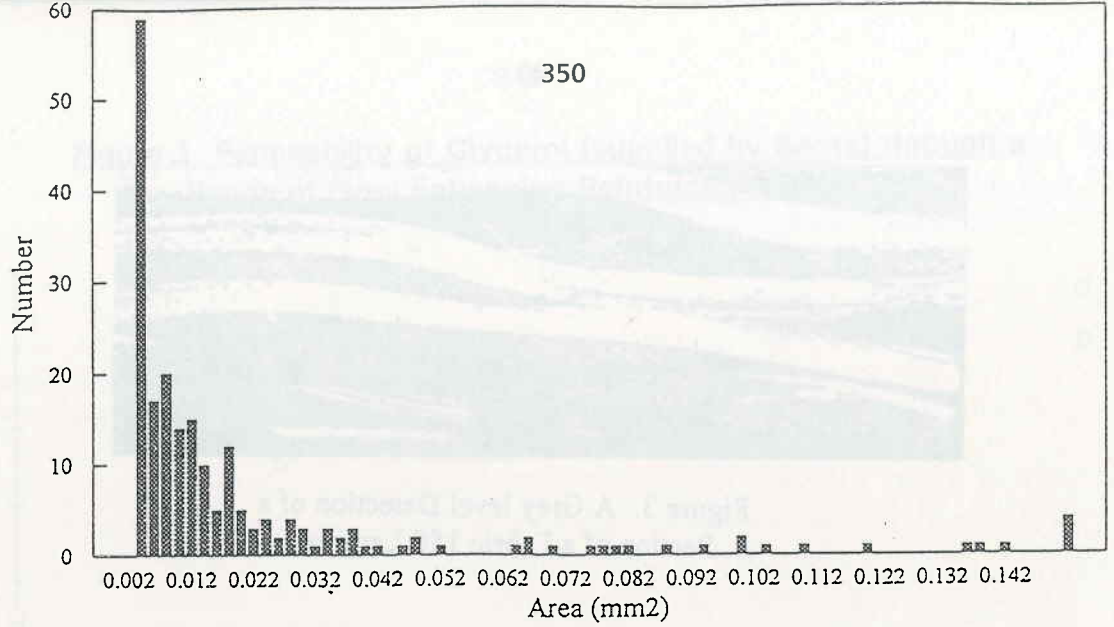

Figure 6a. Histogram of Zone Area in the Twill Laminate

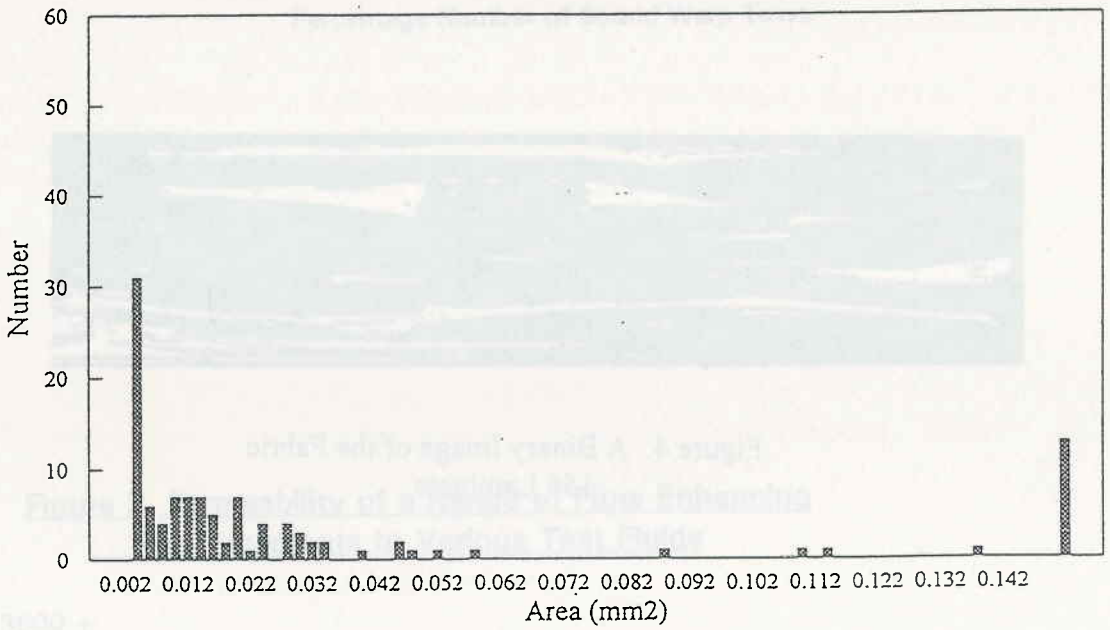

Figure 6b. Histogram of Zone Area in the 156 Laminate

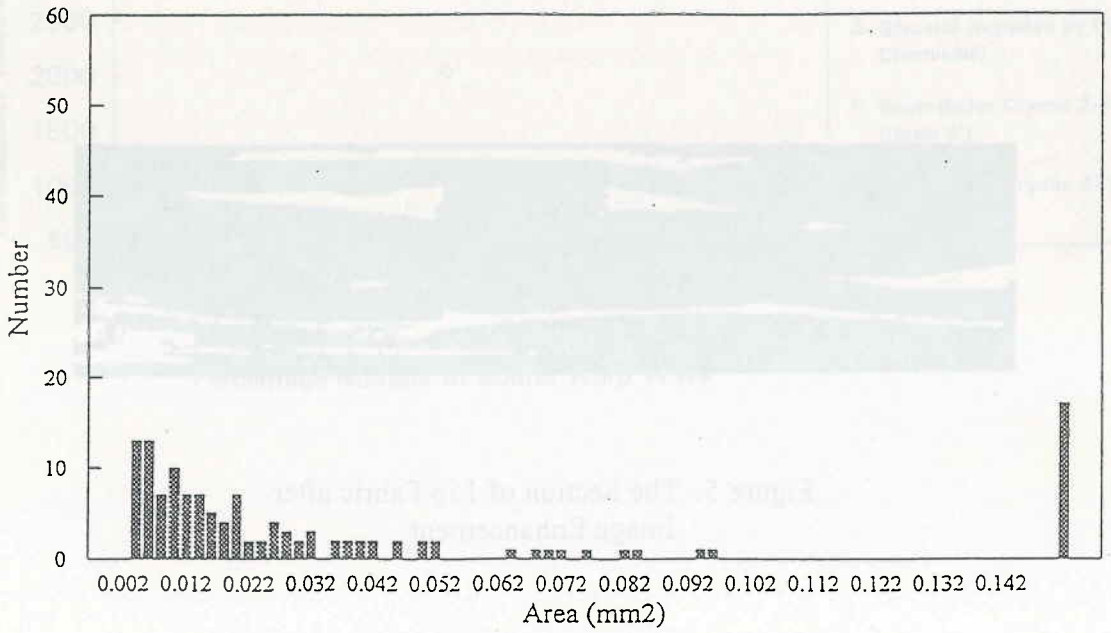

Figure 6c. Histogram of Zone Area in the 126 Laminate

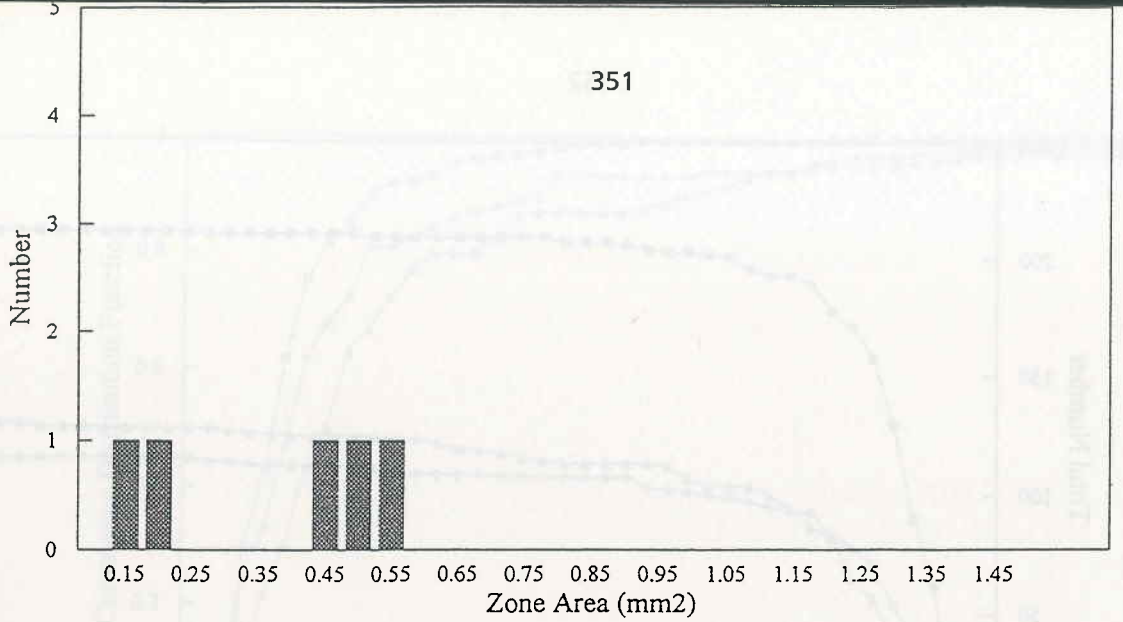

Figure 7a. Histogram of the Large Flow Areas in the Twill Laminate

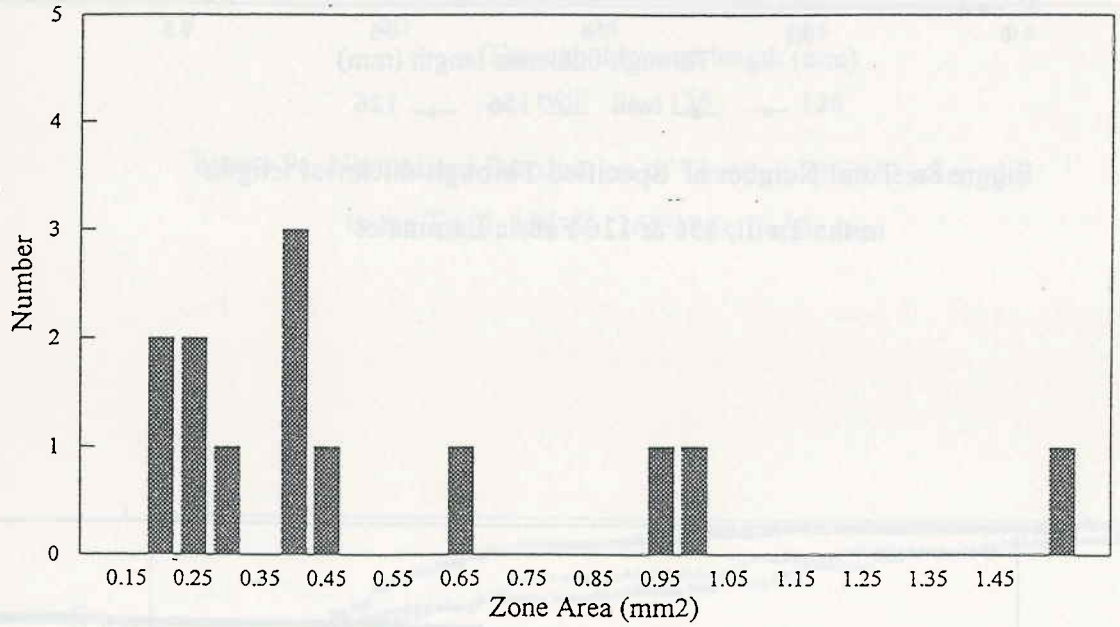

Figure 7b. Histogram of the Large Flow Areas in the 156 Laminate

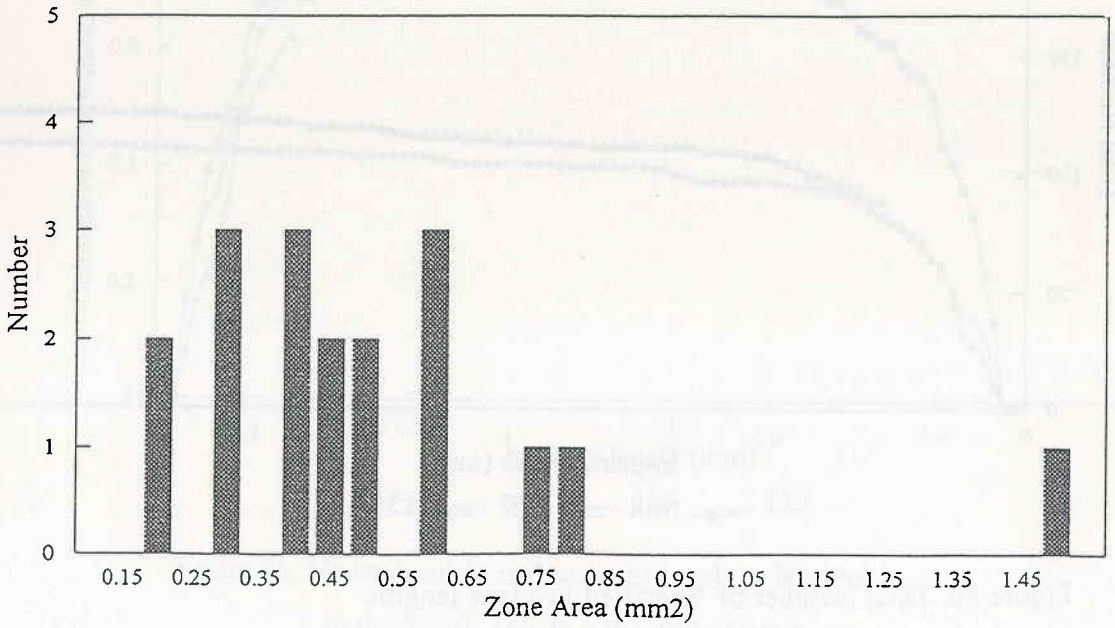

Figure 7c. Histogram of the Large Flow Areas in the 126 Laminate

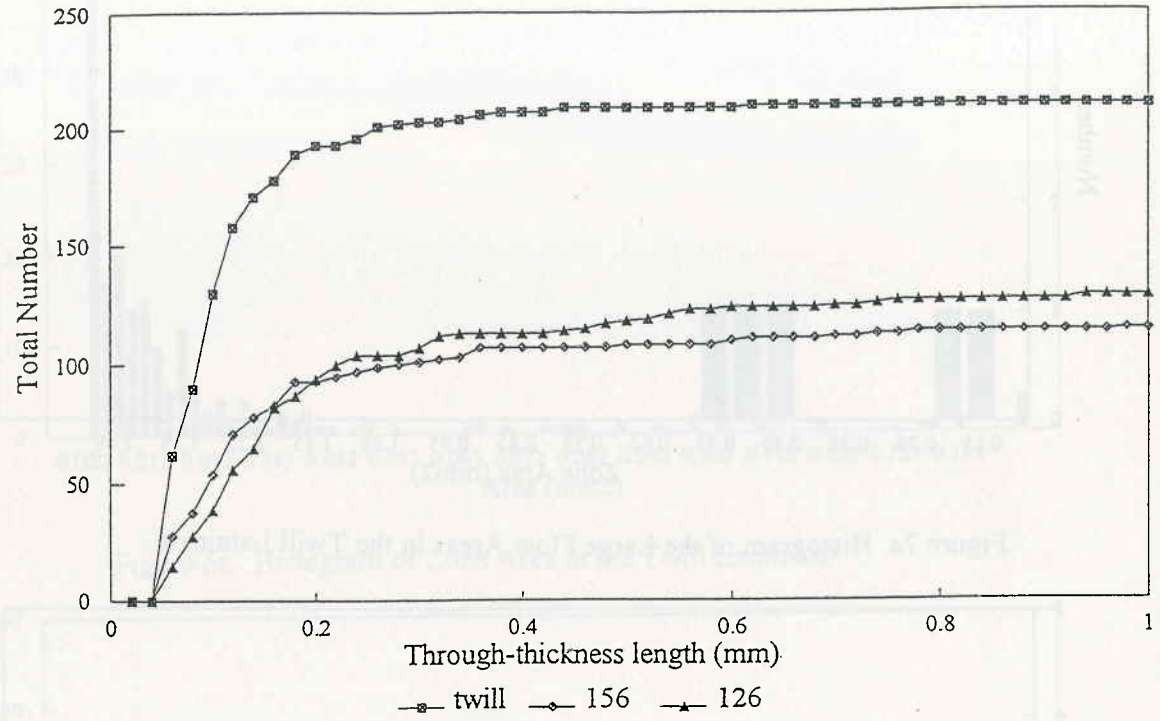

Figure 8a. Total Number of Specified Through-thickness lengths in the Twill, 156 & 126 Fabric Laminates

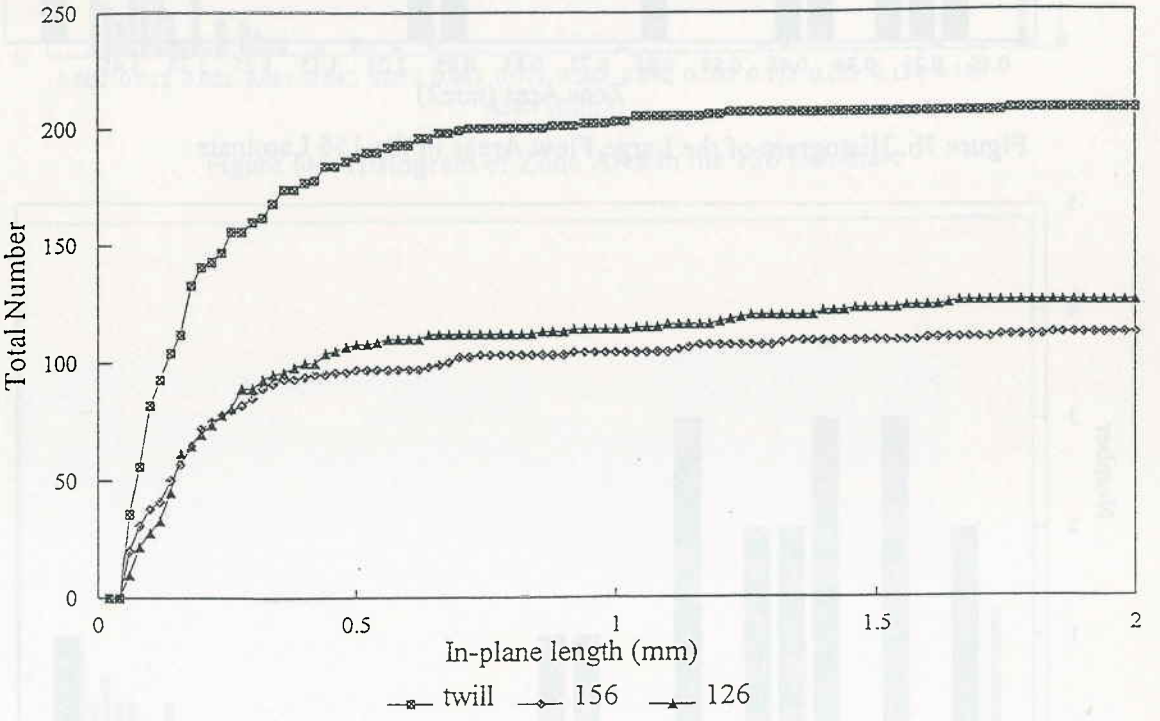

Figure 8b. Total Number of Specified In-plane lengths in the Twill, 156 & 126 Fabric Laminates

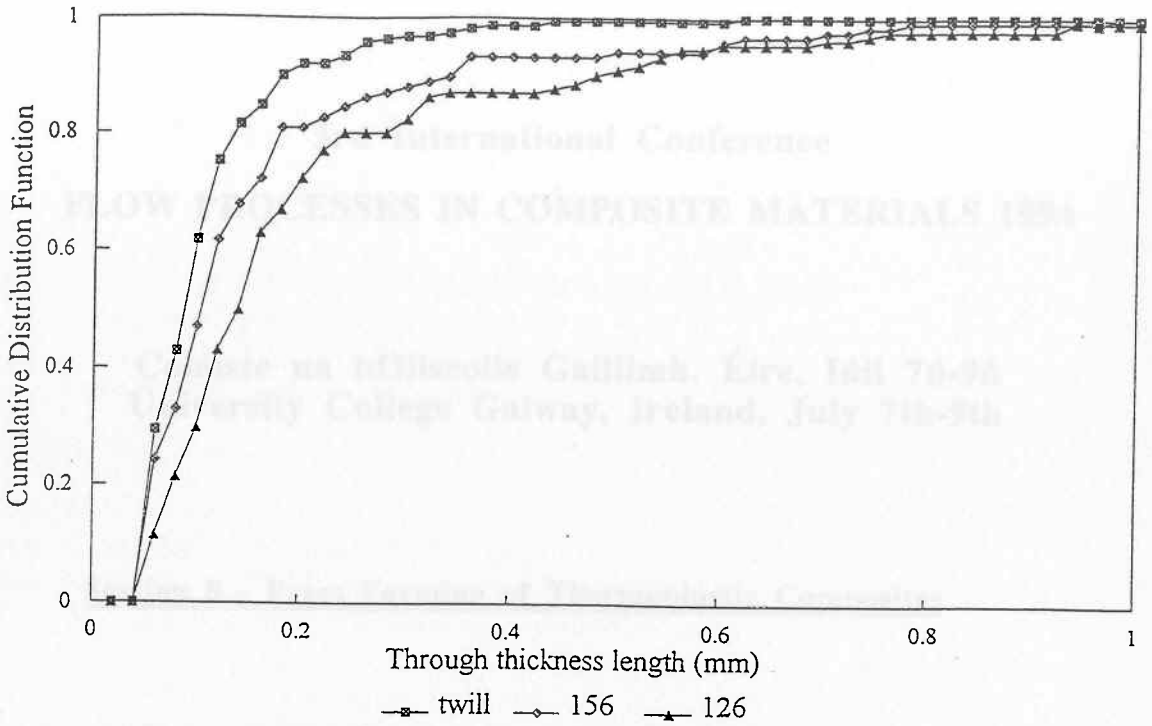

Figure 9a. Normalised Distribution of Through-Thickness lengths in the Twill, 156 & 126 Fabric Laminates

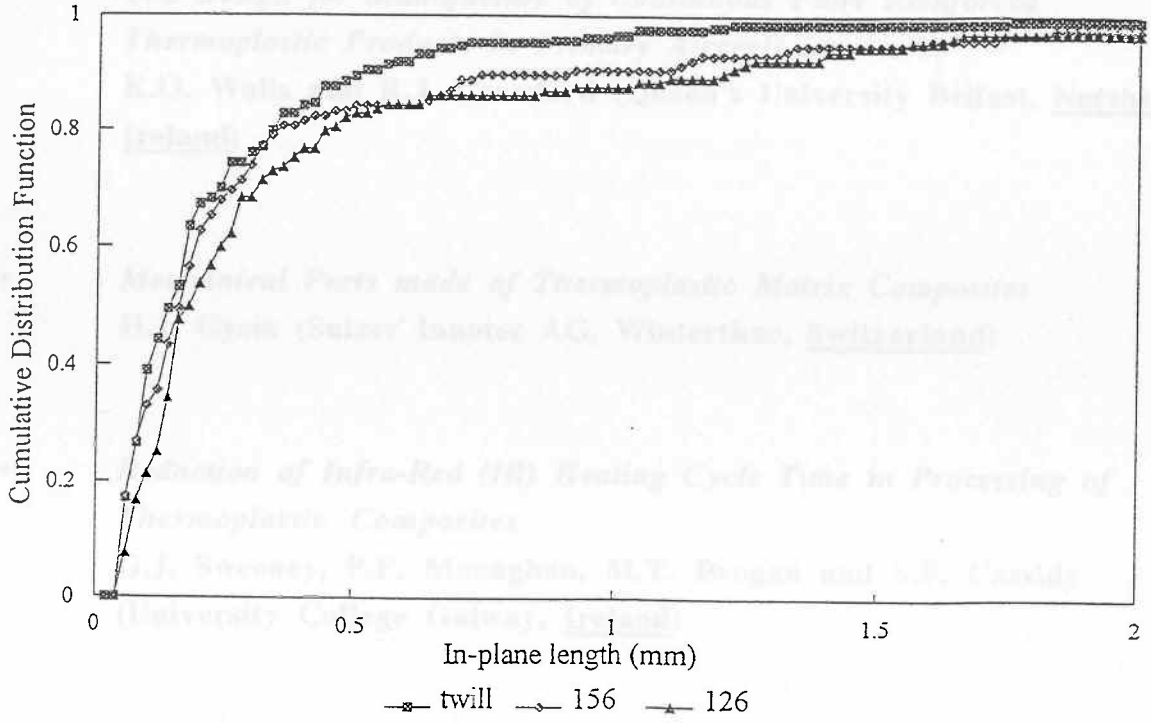

Figure 9b. Normalised Distribution of In-plane lengths in the Twill, 156 & 126 Fabric Laminates